Spatiotemporal Quantification of Lithium both in Electrode and in Electrolyte with Atomic Precision via Operando Neutron Absorption

Harks, Peter Paul R.M.L.; Verhallen, Tomas W.; George, Chandramohan; van den Biesen, Jan Karel ; Liu, Qian; Wagemaker, Marnix; Mulder, Fokko M.

DOI
10.1021/jacs.9b05993

Publication date
2019

Document Version
Final published version

Published in
Journal of the American Chemical Society

JACS JOURNAL OF THE AMERICAN CHEMICAL SOCIETY
Article
Cite This: J. Am. Chem. Soc. 2019, 141, 14280−14287
pubs.acs.org/JACS

Spatiotemporal Quantification of Lithium both in Electrode and in Electrolyte with Atomic Precision via Operando Neutron Absorption

Peter-Paul R. M. L. Harks,[†,‡] Tomas W. Verhallen,[∥,‡] Chandramohan George,[∥,§] Jan Karel van den Biesen,[∥] Qian Liu,[∥] Marnix Wagemaker,[∥] and Fokko M. Mulder*[,†]

[†]Materials for Energy Conversion and Storage (MECS), Department of Chemical Engineering, Delft University of Technology, P.O. Box 5045, 2600 GA Delft, The Netherlands

[∥]Department of Radiation Science and Technology, Delft University of Technology, Mekelweg 15, 2629 JB, Delft, The Netherlands

[§]Dyson School of Design Engineering, Imperial College London, SW7 2AZ London, United Kingdom

Supporting Information

ABSTRACT: The commercial uptake of lithium−sulfur (Li-S) batteries is undermined by their rapid performance decay and short cycle life. These problems originate from the dissolution of lithium polysulfide in liquid electrolytes, causing charge and active material to shuttle between electrodes. The dynamics of intractable polysulfide migration at different length scales often tend to escape the probing ability of many analytical techniques. Spatial and temporal visualization of Li in Li-S electrodes and direct mechanistic understanding of how polysulfides are regulated across Li-S batteries starting from current collector and active layer coating to electrode−electrolyte interface are still lacking. To address this we employ neutron depth profiling across Li-S electrodes using the naturally occurring isotope, ^{6}Li, which yields direct spatial information on Li-S electrochemistry. Using three types of Li-S electrodes, namely, carbon−sulfur, carbon−sulfur with 10% lithium titanium oxide (LTO), and carbon−sulfur with LTO membrane, we provide direct evidence for the migration, adsorption, and confinement of polysulfides in Li-S cells at work. Our findings further provide insights into the dynamics of polysulfide dissolution and re-utilization in relation to Li-S battery capacity and longevity to aid rational electrode designs toward high-energy, safe, and low-cost batteries.

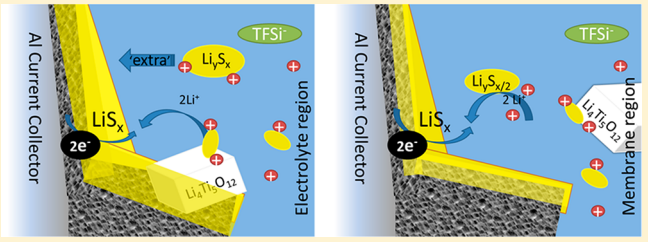

INTRODUCTION

Although clean energy sources are transforming the energy landscape, sustainable power sources are intrinsically intermittent and unable to match supply and demand.[1−4] Therefore, electrochemical energy storage has become paramount to stabilize the grid and mitigate this mismatch.[1,5] To this end, developing safe and cost-effective rechargeable batteries is necessary to lay the foundation, and among the various battery chemistries available today, the high theoretical energy density (2600 Wh/kg), natural abundancy of sulfur (∼2.9%), environmental benignity (low toxicity), and low cost make lithium−sulfur (Li-S) batteries highly attractive alternatives to supersede the current Li ion technology.[6−8]

Despite these advantages, the Li-S battery system suffers from rapid capacity fading and poor round-trip efficiency,[6,7] which seem inherently linked to the material properties of sulfur, i.e., dissolution of the intermediate lithium polysulfide species in the battery electrolyte and Li metal corrosion via polysulfide accumulation.[6,7] The discharge curve of a Li-S battery consists of a high (∼2.3 V) and a low (∼2.0 V) voltage plateau, attributed to a solid (S_8) → liquid (Li_2S_x) → solid (Li_2S_2/Li_2S) process with a gradual decrease in the sulfur chain length. The high plateau is ascribed to the reduction of the cyclic S_8 ring to soluble long-chain polysulfides (Li_2S_x, $4 < x < 8$), while the low voltage plateau is believed to correspond to further reduction of polysulfides to solid Li_2S_2/Li_2S.[9,10] Although sulfur has an extremely low electronic conductivity, which can render it unsuitable as an active material in the traditional sense, the redox process is enabled owing to the limited but sufficient solubility in organic electrolytes of elemental sulfur and the high solubility of electrochemically produced polysulfides,[7] which in part circumvents the limitation of low electronic conductivity of bulk sulfur.[8,11] However, a conductive matrix, most commonly carbon, is required to provide a pathway for electrons and reaction sites, such that the migrated Li ions can shorten the sulfide backbone until the solid product Li_2S is formed.[12]

The "solid−liquid−solid" mode of operation (in liquid electrolyte cells) inevitably incurs a number of issues. Since the intermediate products are dissolved in electrolytes, the active material is no longer confined to the electrode region and is able to migrate to the anode, where it can undergo parasitic reactions. This not only limits the practical performance of Li-S batteries but is the root cause for battery self-discharge and capacity decay.[13]

Received: June 12, 2019
Published: August 25, 2019

The active material migration from cathode to Li anode or shuttling between electrodes must be restrained in order to achieve a reasonable capacity. A common approach is to use electrolyte additives that passivate the anode surface, such as lithium nitrate ($LiNO_3$).[14] Through chemical reaction with S and Li, $LiNO_3$ incurs the formation of a passivating layer on the Li anode. This layer prevents Li metal from being directly exposed to polysulfides, while allowing Li-ion conduction, due to ion-conductive Li_3N species.[15] However, morphological changes during cyclic Li re-deposition cause repetitive breakdown of the passivating layer, resulting in continuous consumption of the $LiNO_3$.[16] Another potential bottleneck is that, although $LiNO_3$ has a sufficient electrochemical stability window that covers the operating potential limits of Li-S batteries, discharging below 1.7 V reduces the $LiNO_3$ at the cathode, adversely affecting the battery performance.[14,17] More importantly, this additive alone cannot inhibit the active material from diffusing out of the electrode region.

Aimed at avoiding active material loss, efforts were focused on physically encapsulating the sulfur active material within hollow carbon structures. Yet the weak interaction between carbon and polysulfide yielded little improvement in terms of cycle life, especially when benchmarked against the current Li-ion cells.[11,18] Recently, chemical bonding strategies for immobilizing polysulfides have been developed,[19] which are based on the strong interactions between polar functional groups and polysulfides.[19−21] Functional groups (e.g., oxygen, boron, nitrogen, and sulfur) are introduced to electrodes via the conductive additive (carbon matrix) or by dispersing polymer or (transition) metal oxide additives (e.g., TiO_2 and $Li_4Ti_5O_{12}$).[22] Their addition considerably improved the performance of Li-S batteries, particularly with increased battery capacity and prolonged cycle life.[23,24] The beneficial effects are attributed to their high polarity, which should yield a high chemical affinity toward polysulfide species.[25] Yet, to date, there is a lack of direct experimental evidence for polysulfide migration and confinement (spatiotemporally resolved) in realistic Li-S batteries.

Among the reasons for this lack is the challenge of studying light ions, such as lithium, using methods based on X-rays or electrons,[26−29] due to the intrinsic difficulties in selectively detecting Li in battery electrode environments. For example, in situ diffractometric techniques are indispensable for understanding the formation of crystalline Li_2S and Li_2S_2 through disproportionation in both electrode and glass fiber separator.[12,30] Yet, the non-crystalline polysulfide chains and nanocrystalline particles cannot be resolved.[12,30,31] Alternatively, inelastic methods based on photon absorption, i.e., UV−vis, XAS, XANES, and RIXS, have been employed, which allow for the study of in operando observations of dissolved polysulfide species.[32−36] In essence, these operando and in situ measurements contribute to a better understanding of polysulfide dynamics, which normally escape the probing ability of ex situ methods and electrochemical testing.[24,26] However, these intense and energetic probes have the potential to increase the risk of samples degradation.[31]

Neutron depth profiling (NDP) allows for the absolute detection of Li with atomic selectivity, independent of the oxidation state or phase. As NDP exploits neutron capture reaction of the lithium-6 isotope, it ensures unique selectivity and intrinsic low noise, whereas the high depth of penetration of neutrons allows for the investigation of practical sample environments, i.e., resembling a commercial cell.[37−40] In this neutron capture reaction, a thermal neutron is absorbed by a ^6Li atom, initiating the formation of two charged particles with a well-defined energy, according to[41,42]

$$^6Li + n_{thermal} \rightarrow {}^3H^+ (2727.88\ keV) + He^{2+} (2055.12\ keV)$$

The nuclear reaction energy released is much larger than the energy of a thermal neutron (~25 meV); hence, the charged particle kinetic energies are constant, independent of the neutron energy. Furthermore, the radiation intensity is low: per second, only 1 out of every 10^{15} ^6Li atoms absorbs a neutron.[37,43] This amount is not significant enough to trigger detrimental effects or deleterious reactions in a 1 cm^2 area electrode, which therefore makes NDP an inherently non-destructive characterization method. A fraction of particles that escape the sample are detected with an energy-sensitive detector, as is illustrated in Figure 1.[27]

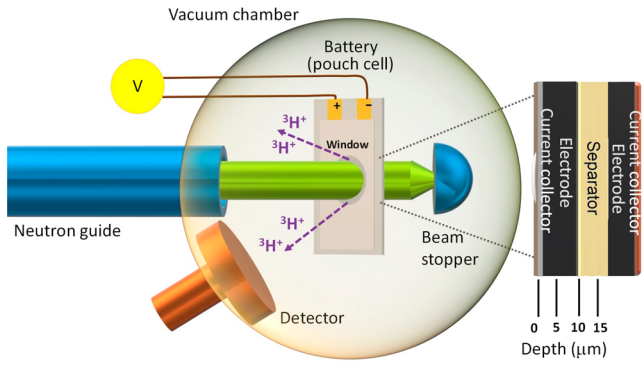

Figure 1. Schematic representation of the operando neutron depth profiling (NDP) setup. The inset shows a cross section of a pouch cell and indicates the electrode region probed. Adapted from ref 27.

The sample-to-detector distance is such that measured particles' (the incoming $^3H^+$ and $^4He^{2+}$) trajectories are almost parallel to the sample−detector axis or perpendicular to both detector and sample plane. The particles lose energy as they travel through the battery electrode materials; that energy is measured by the detector. The energy difference caused by energy lost in the material is a function of the original isotope depth in the sample. Hence, through neutron depth profiling, a cross sectional averaged Li concentration profile as a function of depth is determined, i.e., along the axis perpendicular to the sample surface.[42] Besides this, the ability to measure the ^6Li isotope independent of oxidation state allows for the simultaneous detection of lithium in both electrode and electrolyte, which makes NDP a unique diagnostic tool capable of unraveling the space- and time-dependent lithium density resulting from the complex electrochemical processes taking place across battery electrodes.[37,44,45]

To reveal electrode-wide dynamics that govern polysulfide behavior in Li-S batteries, three groups of electrodes are investigated: a standard carbon−sulfur composite electrode, one standard carbon−sulfur composite electrode with a membrane containing 140 nm $Li_4Ti_5O_{12}$ particles, and an electrode with 10 wt% 140 nm $Li_4Ti_5O_{12}$ particles added.[46] The cells containing these electrodes are hereafter referred to as *standard*, *layered*, and *composite*, respectively. In the layered cell the $Li_4Ti_5O_{12}$ particles are not connected electronically to the current collector, whereas in the composite cell, carbon,

DOI: 10.1021/jacs.9b05993
J. Am. Chem. Soc. 2019, 141, 14280−14287

binder, active material (sulfur), and $Li_4Ti_5O_{12}$ particles are intimately mixed. Through measuring and quantifying the local lithium concentration across the electrode and electrolyte in these cells, direct evidence for Li-containing polysulfide dissolution, migration, and adsorption by metal oxides is presented.

RESULTS AND DISCUSSION

Figure 2 shows the lithium concentration profiles obtained from the pristine cells averaged during an initial 20 min resting time. At zero depth the current collector/battery electrode interface is located. On the right, at high depths, the electrolyte region is located. The lithium concentration in the electrolyte should be close to 1.2 M LiTFSI and $LiNO_3$ in TEGDME. Even though no current was drawn from the cells, Li ions of the battery electrolyte, which has infiltrated the porous network of electrode, are measured. For the standard electrode, indicated by the black squares, a nearly constant lithium concentration of 0.8 M is measured. This is lower than the pure electrolyte concentration, as part of the electrode volume is occupied by intrinsically lithium-free components such as carbon, PDVF binder and active material or the battery separator. At depths beyond 10 μm, the measured Li concentration shows still similar values because it is basically the combination of values from the electrolyte and glass fiber separator. Hence, the total lithium concentration detected was lower. In the other samples, the presence of Li in the lithium titanium oxide (LTO) of the composite electrode and the membrane of the layered cell increases the Li density and therefore the signal in those specific regions, as the Li concentration in pure LTO is over 30 mol/L. The layered cell shows a strong Li increase at ~15 μm depth where the LTO membrane is located. Note that a step transition is not to be expected as a transverse average of the full electrode interface is measured, which is due to the rough interface of the electrode and membrane that leads to a sloping concentration. Similarly, the 10 wt% of LTO in the composite electrode occupies 6% of the volume, thereby increasing the lithium concentration to 1.7 M, indicated by the red spheres, showing a small step at 7 μm, thereby marking the pristine electrode thickness. The Li concentration in the composite electrode converges with increasing depth toward the same concentration as the standard electrode, representing the concentration in the separator. Therefore, the presence of LTO in these electrodes is clearly advantageous for indicating the pristine electrode

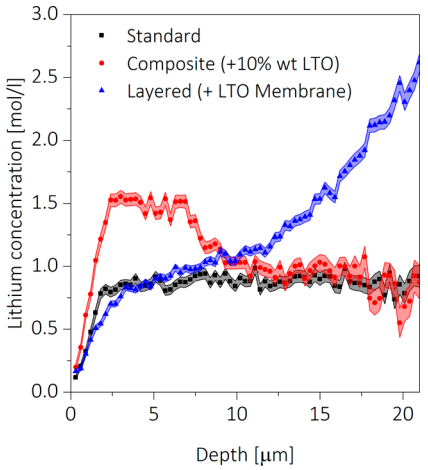

Figure 2. Neutron depth profiling averages of the measurements obtained for pristine cells during the rest period before discharge of three different electrodes. The end of the aluminum current collector/window is at 0 μm depth, from which the porous electrode starts. The error bars increase with depth, as the subtracted background is larger for lower energies; hence, the signal-to-noise ratio decreases while the measurement uncertainty increases.

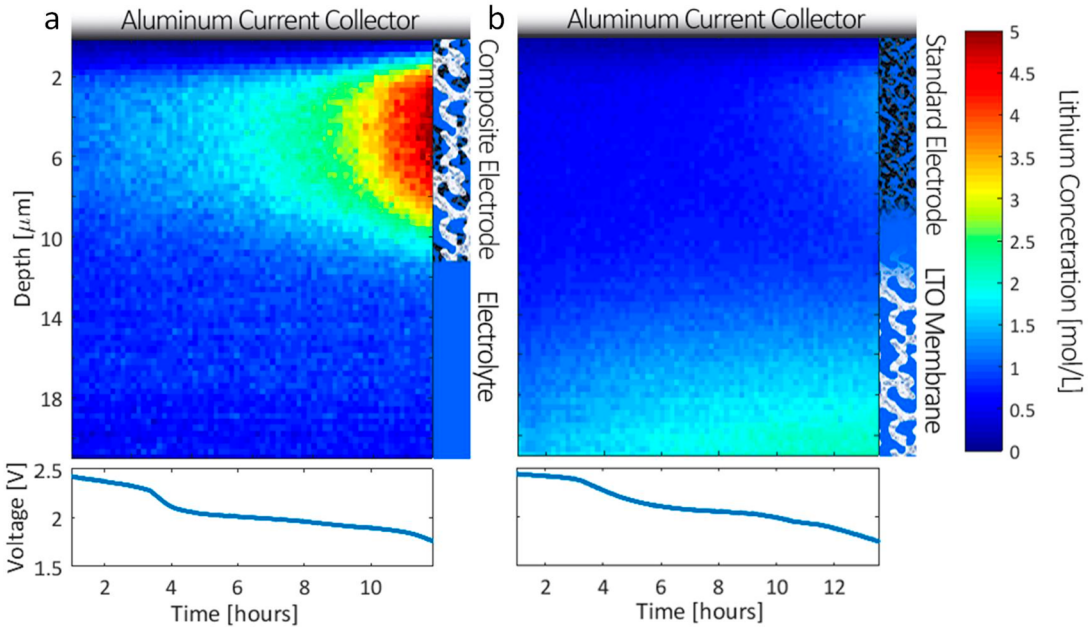

Figure 3. Operando NDP results. Color contour images show the increase in lithium concentration with time versus depth at a constant current discharge; the initial signal of electrolyte and LTO has been subtracted. The aluminum current collector/window is at the top of the plot, whereas the electrolyte (and membrane) are found below. (a) Composite electrode and (b) layered electrode containing a standard CS electrode and LTO membrane.

DOI: 10.1021/jacs.9b05993
J. Am. Chem. Soc. 2019, 141, 14280−14287

thickness, thus enhancing the ability to monitor the location of Li upon reduction of sulfur during battery discharge.

As we focus on the role of LTO (metal oxide) in relation to polysulfide confinement and utilization, the results obtained on the standard electrode can be found in the Supporting Information, Figure S3. The results on the cells (layered and composite) are shown in Figure 3. These color contour images show lithium concentration versus time (horizontal) and electrode depth (vertical) during Li-S battery discharge, and it can be noticed that the Li concentration increases as the batteries are discharged. To remove the contribution of the pristine electrolyte, the concentration of the standard cell (black line in Figure 2) has been subtracted. This correction highlights the change in lithium concentration over time (during discharge) both in the electrode and in the electrolyte.

The bottom panels indicate the cell voltage versus Li. The discharge voltage and plateaus are characteristic of the curve of a Li-S battery. The battery discharge cutoff voltage was set to 1.7 V, in order to prevent electrochemical activity of LTO as well as decomposition of $LiNO_3$. Therefore, the recorded lithium concentration increase is solely due to the electrochemical activity of sulfur forming soluble and solid discharge products, i.e., polysulfide species. At the end of discharge a high lithium concentration is attained in this electrode, providing an indirect evidence of solid deposits accumulating on the carbon matrix. As a result, the electrode layer thickness increases during discharge, reaching 11 μm at the end. This is a 50% increase when compared to Figure 2, where the original layer thickness was deduced from the LTO additive. Previous reports indicate a volume difference between the pristine and lithiated phases of 80%.[47] This observation proves that even though the active material is precipitating from soluble products, the solid deposits are able to strain the carbon matrix, which is in line with previous results obtained by Tonin et al. using tomography.[48]

Figure 3b shows the layered cell, a standard electrode with an LTO membrane. The increased lithium concentration due to the LTO membrane at depths above 10 μm is obvious, and lithiation of the electrode region itself does not progress as significantly as in the composite electrode, even though the same C-rate is applied. Especially in the first half of the discharge there is no visible concentration increase in the electrode region; however, there is a pronounced concentration increase within the LTO membrane. This means that a large fraction of the oxidized Li and reduced sulfur is actually stored within the membrane instead of the electrode region at depths, i.e., below 12 μm. We can safely rule out the possibility of the intercalation or lithiation of LTO particles, as the cell potential is well above the 1.55 V, where intercalation in LTO occurs. Therefore, it can be rationalized that the accumulation of Li in the LTO membrane is not a result of an electrochemical process within the LTO region but is due to the adsorption of Li polysulfides that are produced in the electronically conductive electrode region and then concentrate within the LTO membrane. In other words, they migrate from the electrode region and are confined within the LTO membrane, apparently preventing subsequent Li migration to the anode. This is direct evidence for the ability of LTO to bond the dissolute Li-polysulfide species. In the second half of discharge, after 8 h, the electrode region (<12 μm) does show an increase in lithium concentration. This lithiation might result from low solubility solid products, which deposit on the carbon matrix. This deposition can only occur when electrons are supplied, and this process is therefore restricted to the electrode region. However, the concentration of lithium in the LTO membrane does not decrease, which indicates that the absorbed species are relatively stable and do not re-dissolve to complete the reaction at the end of discharge. Hence, the final concentration attained in the carbon−sulfur electrode with LTO membrane is much lower, which also corroborates its low capacity. This can explain why a Li-S electrode design involving cathode interlayers offers sub-optimal battery performance, if such an interlayer does not provide high electron conductivity or other properties aiding the re-dissolution and reduction of polysulfides. Hence it appears that lithiation proceeds sequentially in the available regions, i.e., in the electrode and electrolyte/membrane region.

To further explore this behavior, the counts from the two different regions in the cell are summed; the region from 0 to 12 μm represents the entire carbon matrix (standard carbon−sulfur or composite) available in electrodes for lithiation, and the region from 12 to 28 μm encompasses the measurable part of the electrolyte or the membrane only. Simultaneously this increases measurement statistics. Next the measured Li concentration increase, integrated over these two separate regions, is related to the current that was retrieved from the battery during discharge, which provides information on the diffusion of lithium polysulfides.

In a conventional intercalation-type battery, the ratio between lithiation and the obtained current should be 1 for the electrode region. This is because for the amount of negative charge produced per second (current) from the battery, the same amount of positive charge (Li ions) should be inserted into the positive electrode (during discharge). Similarly, a ratio of 1 in the case of a Li-S battery means the polysulfide shuttle is completely stopped, as for every electron a lithium is stored in the electrode, with no lithium diffusing into the electrolyte via dissolution. It should be noted that the ratio for the electrode and electrolyte combined also can be lower than 1, as a significant part of the electrolyte is not probed by this method and therefore polysulfides can diffuse out of the measured area.

During the initial stages of discharge, at the first plateau at 2.5−2.3 V, the current divided by the lithiation speed is indeed lower than 1. Here, for both types of electrodes, the lithium increase is slower than expected based on the applied current in the total measurable domain, as shown in Figure 4. This, in line with Li concentration profiles in Figure 3, can be explained by diffusion of Li_2S_n polysulfide species. In this voltage range, highly soluble polysulfides are formed and driven out of the electrode by their concentration gradient. The corresponding increase in Li concentration in both cells spreads over an extended electrolyte area, and therefore the change in Li concentration does not supersede the measurement error inside the probed area. Although the increase in lithium concentration is lower than expected due to the diffusion of polysulfide for both cells, the regions that contain LTO (the electrode and membrane) do exhibit lithiation. In Figure 4a, the composite electrode shows significant electrochemical activity, whereas the electrolyte region barely changes. Even more obvious is the change in the membrane region of the layered cell, Figure 4b. Here, because of the high LTO concentration (85 wt%) in the membrane, more surface area for adsorption is available within the LTO membrane, which is why lithiation proceeds more readily at this stage of discharge. As the cell potential forbids electrochemical activity of the

DOI: 10.1021/jacs.9b05993
J. Am. Chem. Soc. 2019, 141, 14280−14287

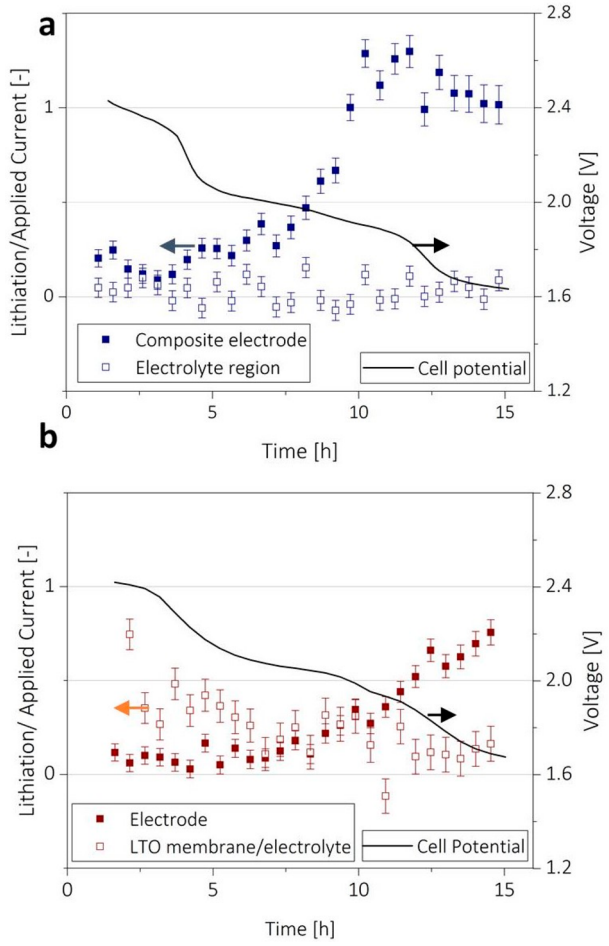

Figure 4. Regional lithiation defined as the Li concentration increase per time unit divided by the current and plotted versus discharge time. Blue symbols in (a) indicate composite electrode cell and red symbols in (b) indicate the standard electrode with membrane; filled squares indicate electrode region whereas open spheres denote electrolyte and electrolyte/membrane regions. Data have been binned; error bars reflect the spread in the data set of one point.

LTO, the sole explanation for the observed lithiation is adsorbed polysulfide species—a direct indication that indeed LTO can retain lithium−sulfur-based solutes.

In the second stage of discharge, when the voltage reaches the 2 V plateau, a clear shift is seen. The composite electrode shows a sudden increase in lithiation speed halfway through the second plateau; the relative lithiation even exceeds 1. This reveals that solid compounds are formed, rapidly consuming the polysulfide species present in the electrolyte in the porous network of the electrode as well as on the surface of the LTO particles. Together with (two) Li ions from the electrolyte, these species are reduced to insoluble products, which are subsequently deposited on the carbon substrate. On top of this process, the lowering of the local polysulfide concentration results in a net influx of these species from the electrolyte reservoir to electrode region, hence leading to the observed "surplus" in lithiation speed. The fact that the observed value surpasses 1 proves that solid sulfur compounds are formed.

In Figure 4b, the layered cell also shows the jump in lithiation speed, albeit somewhat later in the discharge process. Moreover, there is an obvious transition during this voltage plateau, as the activity is moving from the membrane to the electrode region. The contribution to the current of the membrane does not become negative, meaning that the polysulfide species adsorbed during the first stages of discharge are irreversibly trapped in the membrane. The LTO membrane is incapable of supplying the adhered lithium sulfides with electrons; therefore, these polysulfides cannot be further reduced. Furthermore, the lithiation speed is much lower than previously seen for the composite electrode, as the ratio between lithium concentration increase and applied current never reaches 1. A clear indication of soluble products, and consequently capacity, is leaving the measurement scope. This explains the poor capacity obtained from this cell compared to the composite electrode.

To exclude the scenario that significant regions of the carbon matrix are outside of the window, the potential was decreased further (to ∼1.6 V), such that the NO_3 anions become instable, forming lithium oxide according to

$$2Li^+ + NO_3^- + 2e^- \rightarrow Li_2O(s) + NO_2^-$$

This would cause solid deposition of insoluble Li_2O only on the carbon matrix and the exchange of NO_3^- with NO_2^- ions in solution. Therefore, at 1.6 V, the lithiation (normalized to the current) across the electrode regions should be ∼1 for both types of electrodes. This is indeed the case for both cells, proving that the electrochemically active regions are fully within the measurement window.

However, it should be noted that for both electrodes the absorption rate of polysulfides onto the LTO nanopowder does not occur on par with the applied current, which could be due to a lack of available surface sites. We remark that the commercial LTO nanopowder used in this study is not actually designed for this type of application;[46] nevertheless, operando NDP can still capture the polysulfide dynamics across Li-S electrodes containing such LTO and unambiguously establish the proposed Li polysulfide retention mechanism.

Based on our NDP spatiotemporal measurements, we were able to piece together a comprehensive picture of Li-S batteries at work, as sketched in Figure 5. Note that in the cartoon, disproportionation and solid-state reaction pathways have been omitted for clarity and we highlight only what NDP enabled us to measure, which is Li density as a function of electrode depth. Starting from the rest period, where at open-circuit potential (OCP) dissolved S_8 rings are in an equilibrium concentration with the electrolyte, as soon as electrons are supplied, these rings are opened to react and form polysulide complexes. This initiates the progressive dissolution of sulfur active materials, see Figure 5b. These complexes are molecules or possibly ionized to Li^+ and S_n^{2-}. From the results shown in Figures 3 and 4, we can confirm that the soluble polysulfides migrate out of the electrode and are adsorbed at LTO sites. In the case of the layered cell, this migration is observed by a subpar lithiation speed and through the lithium concentration increase in the LTO membrane, which at this voltage can only be attributed to absorbed lithium polysulfide species. This adsorption process also takes place in the composite electrode, but to a smaller extent due to the lower LTO loading. In the last step (Figure 5c) the dissolved polysulfide species react to form solid compounds, which can only occur on a conducting surface, leading to a lithium ion concentration increase in the electrode region. The available polysulfide species are then consumed, which in the composite electrode cell leads to a higher Li concentration, as adsorbed polysulfide can diffuse over the LTO surface to be reduced at the carbon matrix,

DOI: 10.1021/jacs.9b05993
J. Am. Chem. Soc. 2019, 141, 14280−14287

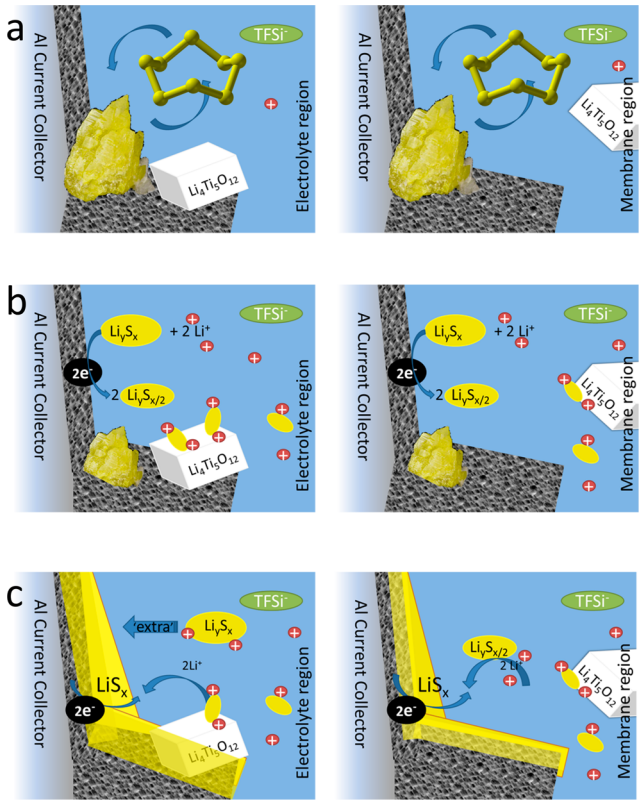

Figure 5. Schematic representation of the Li density present in electrolyte and Li-sulfur compounds within the electrodes and electrolyte during discharge as derived from the operando NDP measurements. (a) Initially Li is in Li-TFSI in the electrolyte and in LTO. The S_8 indicated has a finite solubility, which facilitates electrochemical reduction to Li polysulfides.[7] (b) During discharge, highly soluble Li-S polysulfides are formed with increasing Li-to-S ratios, increased Li density observed in electrolyte, and adsorbed on LTO where present. (c) Further reduction of the lithium polysulfides leads to less-soluble Li_2S_2 deposition on the conducting electrode framework while some Li-S species remain adsorbed on the LTO.

whereas in the CS + LTO membrane electrode (layered) they are contained by the membrane, unable to participate in further reactions. Finally, in the composite electrode, due to the effective conversion of dissolved polysulfide into solid products, the concentration in the electrode area decreases; hence, it becomes thermodynamically favorable for polysulfide species to diffuse from the electrolyte toward the electrode region. This additional flux is registered atop of the reaction necessary to sustain the current.

CONCLUSION

By using neutron depth profiling (NDP), we obtain and present real-time evidence for polysulfide migration during different stages of the Li-S cell discharge process. As NDP enabled us to measure Li concentration in both electrode and electrolyte simultaneously, we also present the first operando evidence of polysulfide adsorption onto metal oxide (LTO). Through comparison of three different electrode configurations, the electrochemical processes, and the diffusional behavior of active material, we have elaborated on the key processes that take place in Li-S batteries: (i) Ideal trapping agents are mixed in the electrode matrix and electronically conductive, such that the agent can transfer electrons to the adhered species, thereby providing a catalytic function and aiding polysulfide redox reaction toward solid deposition. Solely trapping of polysulfides, using a metal oxide membrane interlayer, does not necessarily improve the capacity of a Li-S battery. (ii) Even though reversible polysulfide migration during battery (dis)charge is to be anticipated based on the performance of straightforwardly fabricated sulfur−carbon batteries, i.e., cells with no significant polysulfide confinement, here we found direct evidence for the reversibility of this process. (iii) Volume expansion can be in part offset by the dissolution of polysulfide; however, the formation of solid products can strain the host matrix significantly. We therefore emphasize that, for the design of commercial sulfur batteries, finding the optimum ratio between sulfur and adsorbing additive for dissolution, confinement, and re-utilization of polysulfide is indispensable. Thus, our findings enabled by spatiotemporal NDP measurement can guide the design of both Li-S electrode and cell with negligible capacity fade and improved life, which is the crucial step toward realizing commercially viable Li-S batteries.

METHODS

Electrodes were prepared by the conventional slurry-based process. A slurry was prepared by mixing sulfur (Sigma-Aldrich), Ketjen black (Akzo Nobel), KS4 graphite (Timcal), and PVDF (Kynar Flex) in a weight ratio of 60:15:10:15 in *N*-methyl pyrolidone (NMP, Sigma-Aldrich). For the LTO-containing electrodes, 10 wt% pure LTO (particle size ∼150 nm, Süd-Chemie) was applied to the mixture, at the expense of sulfur. The slurry was then cast onto Al foil using a doctor blade. LTO membranes were prepared by mixing LTO and PVDF in a weight ratio of 85:15, without a conductive additive. The semiconducting LTO, with intrinsic low electronic conductivity and low operating potential, should prevent electrochemical energy storage in the membrane, thereby solely showcasing the polysulfide confinement ability. The slurry was subsequently cast on a glass substrate and then immersed in demineralized water, which produced a free-standing membrane which is self-detachable from the substrate. This membrane is then dried and stacked upon a standard carbon sulfur electrode; the two are not pressed or calendared to avoid electronic contact. SEM images of electrode cross sections are supplied in the Supporting Information.

The cells were assembled inside an Ar-filled glovebox with oxygen and water content less than 1 ppm. Lithium foil was used as the counter and reference electrodes, combined with a glass fiber (Whatman) separator (∼250 μm thick) and the working electrodes to make up the cell. As electrolyte a solution of 1 M LiTFSI in TEGDME was used, with 1 wt% $LiNO_3$ additive. Prior to electrochemical measurements, the electrodes were briefly dried at 60 °C in a vacuum oven. After assembly the cells were left for 1 h to allow soaking and stabilization of the OCP before testing.

The galvanostatic cycling experiments were performed with a programmable Maccor 4000 series galvanostat. The cells were discharged to 1 V and charged to 3.8 V vs Li^+/Li^0 at various C-rates (1C = 1675 mA·g^{-1}). The cells reached capacity values of 0.24 and 0.205 mAh at 1.7 V for the composite and layered cell, respectively.

Pouch cells or coffee bag cells, similar to those used in industrial practice, were used in the neutron depth profiling setup.[49,50] Their simplicity allows for straightforward sealing of the current collector with the pouch material, enabling it to be used as a window for the ^3H ions.[51,52] A window diameter of 16 mm was used, while electrodes were cast with a 13 mm diameter to facilitate alignment. The use of the low vapor pressure TEGDME solvent allows for operation in the vacuum chamber of the NDP experiment.[53]

The NDP experiments were performed at the dedicated beamline at Reactor Institute Delft.[37,44] In the experiments, the tritons, $^3H^+$, formed by the neutron capture reaction are counted versus particle kinetic energy for 10 min per spectrum (collection time). The alpha

DOI: 10.1021/jacs.9b05993
J. Am. Chem. Soc. 2019, 141, 14280−14287

particles do not penetrate the aluminum current collector.[27] Every $^{3}H^{+}$ counted reflects one lithium (^{6}Li), while the associated energy reflects the depth of origin on the trajectory toward the detection. The energy lost per unit of length, or the stopping power, is calculated by taking into account all electrode constituents and their volume ratios.[37] All cell constituents are of commercial origin; there is no reason to expect any differences in $^{7}Li/^{6}Li$ ratios. Despite the high capacity and associated volume change of sulfur (80%),[47,48] a constant energy-to-depth conversion is used, rationalized by the mere minor differences in the stopping power between the lithiated sulfur and the pristine material, especially in relation to the other constituents, see Figure S2. It should be noted that all constituents are of similar stopping power, and hence a change in volume ratio should not significantly alter the depth interpretation; see details in the Supporting Information. Together the depth, sample area, measured beam intensity, and known measurement efficiency allow for the translation of $^{3}H^{+}$ counts into Li concentration as shown in Figure 2.[27]

■ ASSOCIATED CONTENT

Supporting Information

The Supporting Information is available free of charge on the ACS Publications website at DOI: 10.1021/jacs.9b05993.

Electrode fabrication, including SEM views (Figure S1), calculated stopping power of all cell constituents (Figure S2), and NPD result of the standard electrode (Figure S3) (PDF)

■ AUTHOR INFORMATION

Corresponding Author

*f.m.mulder@tudelft.nl

ORCID

Tomas W. Verhallen: 0000-0002-8473-4321
Chandramohan George: 0000-0003-2906-6399
Marnix Wagemaker: 0000-0003-3851-1044
Fokko M. Mulder: 0000-0003-0526-7081

Author Contributions

‡Peter-Paul R.M.L. Harks and Tomas W. Verhallen contributed equally.

Notes

The authors declare no competing financial interest.

■ ACKNOWLEDGMENTS

We acknowledge financial support for this research from ADEM, A green Deal in Energy Materials of the Ministry of Economic Affairs of The Netherlands (www.adem-innovationlab.nl). C.G. acknowledges FlexBatteries (grant agreement no. 704659) from Marie Skłodowska-Curie action H2020-MSCA-IF-2015.

■ REFERENCES

(1) Mulder, F. M. Implications of diurnal and seasonal variations in renewable energy generation for large scale energy storage. *J. Renewable Sustainable Energy* **2014**, *6* (3), 033105.

(2) Dunn, B.; Kamath, H.; Tarascon, J.-M. Electrical Energy Storage for the Grid: A Battery of Choices. *Science* **2011**, *334* (6058), 928–935.

(3) Armaroli, N.; Balzani, V. Towards an electricity-powered world. *Energy Environ. Sci.* **2011**, *4* (9), 3193–3222.

(4) Aggeler, D.; Canales, F.; Zelaya, H.; Parra, D. L.; Coccia, A.; Butcher, N.; Apeldoorn, O. Ultra-fast DC-charge infrastructures for EV-mobility and future smart grids, 2010 IEEE PES Innovative Smart Grid Technologies Conference Europe (ISGT Europe), Oct 11–13, 2010; pp 1–8.

(5) Keshan, H.; Thornburg, J.; Ustun, T. S. Comparison of lead-acid and lithium ion batteries for stationary storage in off-grid energy systems, 4th IET Clean Energy and Technology Conference (CEAT 2016), Nov 14–15, 2016; pp 1–7.

(6) Kang, H. S.; Park, E.; Hwang, J. Y.; Kim, H.; Aurbach, D.; Rosenman, A.; Sun, Y. K. A Scaled-Up Lithium (Ion)-Sulfur Battery: Newly Faced Problems and Solutions. *Adv. Mater. Technol.* **2016**, *1* (6), 1600052.

(7) Harks, P. P. R. M. L.; Robledo, C. B.; Verhallen, T. W.; Notten, P. H. L.; Mulder, F. M. The Significance of Elemental Sulfur Dissolution in Liquid Electrolyte Lithium Sulfur Batteries. *Adv. Energy Mater.* **2017**, *7* (3), 1601635.

(8) Manthiram, A.; Fu, Y.; Chung, S.-H.; Zu, C.; Su, Y.-S. Rechargeable Lithium–Sulfur Batteries. *Chem. Rev.* **2014**, *114* (23), 11751–11787.

(9) Zhao, E. Y.; Nie, K. H.; Yu, X. Q.; Hu, Y. S.; Wang, F. W.; Xiao, J.; Li, H.; Huang, X. J. Advanced Characterization Techniques in Promoting Mechanism Understanding for Lithium-Sulfur Batteries. *Adv. Funct. Mater.* **2018**, *28* (38), 1707543.

(10) Fang, R.; Zhao, S.; Sun, Z.; Wang, D.-W.; Cheng, H.-M.; Li, F. More Reliable Lithium-Sulfur Batteries: Status, Solutions and Prospects. *Adv. Mater.* **2017**, *29* (48), 1606823.

(11) Zhang, S. S. Liquid electrolyte lithium/sulfur battery: Fundamental chemistry, problems, and solutions. *J. Power Sources* **2013**, *231*, 153–162.

(12) Conder, J.; Bouchet, R.; Trabesinger, S.; Marino, C.; Gubler, L.; Villevieille, C. Direct observation of lithium polysulfides in lithium–sulfur batteries using operando X-ray diffraction. *Nature Energy* **2017**, *2*, 17069.

(13) Cleaver, T.; Kovacik, P.; Marinescu, M.; Zhang, T.; Offer, G. Perspective—Commercializing Lithium Sulfur Batteries: Are We Doing the Right Research? *J. Electrochem. Soc.* **2018**, *165* (1), A6029–A6033.

(14) Aurbach, D.; Pollak, E.; Elazari, R.; Salitra, G.; Kelley, C. S.; Affinito, J. On the Surface Chemical Aspects of Very High Energy Density, Rechargeable Li-Sulfur Batteries. *J. Electrochem. Soc.* **2009**, *156* (8), A694–A702.

(15) Park, K.; Goodenough, J. B. Dendrite-Suppressed Lithium Plating from a Liquid Electrolyte via Wetting of Li3N. *Adv. Energy Mater.* **2017**, *7* (19), 1700732.

(16) Liu, M.; Cheng, Z.; Qian, K.; Verhallen, T.; Wang, C.; Wagemaker, M. Efficient Li-Metal Plating/Stripping in Carbonate Electrolytes Using a LiNO3-Gel Polymer Electrolyte, Monitored by Operando Neutron Depth Profiling. *Chem. Mater.* **2019**, *31*, 4564.

(17) Zhang, S. S. A new finding on the role of LiNO3 in lithium-sulfur battery. *J. Power Sources* **2016**, *322*, 99–105.

(18) Chen, R.; Zhao, T.; Wu, F. From a historic review to horizons beyond: lithium–sulphur batteries run on the wheels. *Chem. Commun.* **2015**, *51* (1), 18–33.

(19) Liang, X.; Garsuch, A.; Nazar, L. F. Sulfur cathodes based on conductive MXene nanosheets for high-performance lithium–sulfur batteries. *Angew. Chem.* **2015**, *127* (13), 3979–3983.

(20) Pang, Q.; Liang, X.; Kwok, C. Y.; Nazar, L. F. Advances in lithium–sulfur batteries based on multifunctional cathodes and electrolytes. *Nature Energy* **2016**, *1*, 16132.

(21) Pang, Q.; Liang, X.; Kwok, C. Y.; Kulisch, J.; Nazar, L. F. A Comprehensive Approach toward Stable Lithium–Sulfur Batteries with High Volumetric Energy Density. *Adv. Energy Mater.* **2017**, *7* (6), 1601630.

(22) Rao, D.; Zhang, L.; Wang, Y.-h.; Meng, Z.; Qian, X.; Liu, J.; Shen, X.; Qiao, G.; Lu, R. Mechanism on the Improved Performance of Lithium Sulfur Batteries with MXene-Based Additives. *J. Phys. Chem. C* **2017**, *121*, 11047.

(23) Liu, X.; Huang, J. Q.; Zhang, Q.; Mai, L. Q. Nanostructured Metal Oxides and Sulfides for Lithium-Sulfur Batteries. *Adv. Mater.* **2017**, *29*, 1601759.

(24) Fan, X.; Sun, W.; Meng, F.; Xing, A.; Liu, J. Advanced chemical strategies for lithium–sulfur batteries: A review. *Green Energy & Environment* **2018**, *3* (1), 2–19.

DOI: 10.1021/jacs.9b05993
J. Am. Chem. Soc. 2019, 141, 14280–14287

(25) Qu, Q.; Gao, T.; Zheng, H.; Wang, Y.; Li, X.; Li, X.; Chen, J.; Han, Y.; Shao, J.; Zheng, H. Strong Surface-Bound Sulfur in Conductive MoO2Matrix for Enhancing Li-S Battery Performance. *Adv. Mater. Interfaces* **2015**, *2* (7), 1500048.
(26) Conder, J.; Villevieille, C. Is the Li-S battery an everlasting challenge for operando techniques? *Curr. Opin. Electrochem.* **2018**, *9*, 33−40.
(27) Zhang, X. Y.; Verhallen, T. W.; Labohm, F.; Wagemaker, M. Direct Observation of Li-Ion Transport in Electrodes under Nonequilibrium Conditions Using Neutron Depth Profiling. *Adv. Energy Mater.* **2015**, *5* (15), 1500498.
(28) Zhu, W.; Liu, D.; Paolella, A.; Gagnon, C.; Gariépy, V.; Vijh, A.; Zaghib, K. Application of Operando X-ray Diffraction and Raman Spectroscopies in Elucidating the Behavior of Cathode in Lithium-Ion Batteries. *Front. Energy Res.* **2018**, *6*, 66.
(29) Risse, S.; Jafta, C. J.; Yang, Y.; Kardjilov, N.; Hilger, A.; Manke, I.; Ballauff, M. Multidimensional operando analysis of macroscopic structure evolution in lithium sulfur cells by X-ray radiography. *Phys. Chem. Chem. Phys.* **2016**, *18* (15), 10630−6.
(30) Waluś, S.; Barchasz, C.; Colin, J.-F.; Martin, J.-F.; Elkaïm, E.; Leprêtre, J.-C.; Alloin, F. New insight into the working mechanism of lithium−sulfur batteries: in situ and operando X-ray diffraction characterization. *Chem. Commun.* **2013**, *49* (72), 7899−7901.
(31) Paolella, A.; Zhu, W.; Marceau, H.; Kim, C.-s.; Feng, Z.; Liu, D.; Gagnon, C.; Trottier, J.; Abdelbast, G.; Hovington, P.; Vijh, A.; Demopoulos, G. P.; Armand, M.; Zaghib, K. Transient existence of crystalline lithium disulfide Li2S2 in a lithium-sulfur battery. *J. Power Sources* **2016**, *325*, 641−645.
(32) Patel, M. U. M.; Demir-Cakan, R.; Morcrette, M.; Tarascon, J.-M.; Gaberscek, M.; Dominko, R. Li-S Battery Analyzed by UV/Vis in Operando Mode. *ChemSusChem* **2013**, *6* (7), 1177−1181.
(33) Zhao, E.; Nie, K.; Yu, X.; Hu, Y. S.; Wang, F.; Xiao, J.; Li, H.; Huang, X. Advanced characterization techniques in promoting mechanism understanding for lithium−sulfur batteries. *Adv. Funct. Mater.* **2018**, *28* (38), 1707543.
(34) Gorlin, Y.; Patel, M. U.; Freiberg, A.; He, Q.; Piana, M.; Tromp, M.; Gasteiger, H. A. Understanding the charging mechanism of lithium-sulfur batteries using spatially resolved operando X-ray absorption spectroscopy. *J. Electrochem. Soc.* **2016**, *163* (6), A930−A939.
(35) Pang, Q.; Kundu, D.; Cuisinier, M.; Nazar, L. F. Surface-enhanced redox chemistry of polysulphides on a metallic and polar host for lithium-sulphur batteries. *Nat. Commun.* **2014**, *5*, 4759.
(36) Kavčič, M.; Bučar, K.; Petric, M.; Žitnik, M.; Arčon, I.; Dominko, R.; Vizintin, A. Operando Resonant Inelastic X-ray Scattering: An Appropriate Tool to Characterize Sulfur in Li-S Batteries. *J. Phys. Chem. C* **2016**, *120* (43), 24568−24576.
(37) Verhallen, T. W.; Lv, S.; Wagemaker, M. Operando Neutron Depth Profiling to Determine the Spatial Distribution of Li in Li-ion Batteries. *Front. Energy Res.* **2018**, *6*, 62.
(38) Wang, H.; Downing, R. G.; Dura, J. A.; Hussey, D. S. In Situ Neutron Techniques for Studying Lithium Ion Batteries. In *Polymers for Energy Storage and Delivery: Polyelectrolytes for Batteries and Fuel Cells*; Page, K. A., Soles, C. L., Runt, J., Eds.; ACS Symposium Series*1096*; American Chemical Society: 2012; pp 91−106.
(39) Harks, P. P. R. M. L.; Mulder, F. M.; Notten, P. H. L. In situ methods for Li-ion battery research: A review of recent developments. *J. Power Sources* **2015**, *288*, 92−105.
(40) Wang, J.; Liu, D. X.; Canova, M.; Downing, R. G.; Cao, L. R.; Co, A. C. Profiling lithium distribution in Sn anode for lithium-ion batteries with neutrons. *J. Radioanal. Nucl. Chem.* **2014**, *301* (1), 277−284.
(41) Ziegler, J. F.; Cole, G. W.; Baglin, J. E. E. Technique for determining concentration profiles of boron impurities in substrates. *J. Appl. Phys.* **1972**, *43* (9), 3809−3815.
(42) Whitney, S. M.; Biegalski, S. R. F.; Downing, G. Benchmarking and analysis of 6Li neutron depth profiling of lithium ion cell electrodes. *J. Radioanal. Nucl. Chem.* **2009**, *282* (1), 173.
(43) Tan, C.; Leung, K. Y.; Liu, D. X.; Canova, M.; Downing, R. G.; Co, A. C.; Cao, L. R. Gamma radiation effects on Li-ion battery electrolyte in neutron depth profiling for lithium quantification. *J. Radioanal. Nucl. Chem.* **2015**, *305* (2), 675−680.
(44) Oudenhoven, J. F. M.; Labohm, F.; Mulder, M.; Niessen, R. A. H.; Mulder, F. M.; Notten, P. H. L. In Situ Neutron Depth Profiling: A Powerful Method to Probe Lithium Transport in Micro-Batteries. *Adv. Mater.* **2011**, *23* (35), 4103.
(45) Chen, C.; Oudenhoven, J. F. M.; Danilov, D. L.; Vezhlev, E.; Gao, L.; Li, N.; Mulder, F. M.; Eichel, R.-A.; Notten, P. H. L. Origin of Degradation in Si-Based All-Solid-State Li-Ion Microbatteries. *Adv. Energy Mater.* **2018**, *8* (30), 1801430.
(46) Singh, D. P.; Mulder, F. M.; Wagemaker, M. Templated spinel Li4Ti5O12 Li-ion battery electrodes combining high rates with high energy density. *Electrochem. Commun.* **2013**, *35*, 124−127.
(47) Wang, D.-W.; Zeng, Q.; Zhou, G.; Yin, L.; Li, F.; Cheng, H.-M.; Gentle, I. R.; Lu, G. Q. M. Carbon−sulfur composites for Li-S batteries: status and prospects. *J. Mater. Chem. A* **2013**, *1* (33), 9382−9394.
(48) Tonin, G.; Vaughan, G.; Bouchet, R.; Alloin, F.; Di Michiel, M.; Boutafa, L.; Colin, J.-F.; Barchasz, C. Multiscale characterization of a lithium/sulfur battery by coupling operando X-ray tomography and spatially-resolved diffraction. *Sci. Rep.* **2017**, *7* (1), 2755.
(49) Gustafsson, T.; Thomas, J. O.; Koksbang, R.; Farrington, G. C. The polymer battery as an environment for in situ X-ray diffraction studies of solid-state electrochemical processes. *Electrochim. Acta* **1992**, *37* (9), 1639−1643.
(50) Trask, S. E.; Li, Y.; Kubal, J. J.; Bettge, M.; Polzin, B. J.; Zhu, Y.; Jansen, A. N.; Abraham, D. P. From coin cells to 400 mAh pouch cells: Enhancing performance of high-capacity lithium-ion cells via modifications in electrode constitution and fabrication. *J. Power Sources* **2014**, *259*, 233−244.
(51) Lv, S.; Verhallen, T.; Vasileiadis, A.; Ooms, F.; Xu, Y.; Li, Z.; Li, Z.; Wagemaker, M. Operando monitoring the Lithium spatial distribution of Li-metal anodes. *Nat. Commun.* **2018**, *9*, 2152.
(52) Zhang, X.; van Hulzen, M.; Singh, D. P.; Brownrigg, A.; Wright, J. P.; van Dijk, N. H.; Wagemaker, M. Rate-Induced Solubility and Suppression of the First-Order Phase Transition in Olivine LiFePO4. *Nano Lett.* **2014**, *14* (5), 2279−2285.
(53) Tang, S.; Zhao, H. Glymes as versatile solvents for chemical reactions and processes: from the laboratory to industry. *RSC Adv.* **2014**, *4* (22), 11251−11287.

DOI: 10.1021/jacs.9b05993
J. Am. Chem. Soc. 2019, 141, 14280−14287